Article ID: 1006-8775(2009) 01-0181-11

A CLOUD-RESOLVING MODELING STUDY OF SURFACE RAINFALL PROCESSES ASSOCIATED WITH LANDFALLING TYPHOON KAEMI(2006)

CUI Xiao-peng (崔晓鹏)[1], XU Feng-wen (许凤雯)[2]

(1. Laboratory of Cloud-Precipitation Physics and Severe Storms (LACS), Institute of Atmospheric Physics, Chinese Academy of Sciences, Beijing 100029 China; 2. National Meteorological Center, China Meteorological Administration, Beijing 100081, China)

Abstract: The detailed surface rainfall processes associated with landfalling typhoon Kaemi(2006) are investigated based on hourly data from a two-dimensional cloud-resolving model simulation. The model is integrated for 6 days with imposed large-scale vertical velocity, zonal wind, horizontal temperature and vapor advection from National Center for Environmental Prediction (NCEP) / Global Data Assimilation System (GDAS) data. The simulation data are validated with observations in terms of surface rain rate. The Root-Mean-Squared (RMS) difference in surface rain rate between the simulation and the gauge observations is 0.660 mm h^{-1}, which is smaller than the standard deviations of both the simulated rain rate (0.753 mm h^{-1}) and the observed rain rate (0.833 mm h^{-1}). The simulation data are then used to study the physical causes associated with the detailed surface rainfall processes during the landfall. The results show that time averaged and model domain-mean P_s mainly comes from large-scale convergence (Q_{WVF}) and local vapor loss (positive Q_{WVT}). Large underestimation (about 15%) of P_s will occur if Q_{WVT} and Q_{CM} (cloud source/sink) are not considered as contributors to P_s. Q_{WVF} accounts for the variation of P_s during most of the integration time, while it is not always a contributor to P_s. Sometimes surface rainfall could occur when divergence is dominant with local vapor loss to be a contributor to P_s. Surface rainfall is a result of multi-timescale interactions. Q_{WVE} possesses the longest time scale and the lowest frequency of variation with time and may exert impact on P_s on longer time scales. Q_{WVF} possesses the second longest time scale and lowest frequency and can explain most of the variation of P_s. Q_{WVT} and Q_{CM} possess shorter time scales and higher frequencies, which can explain more detailed variations in P_s.

Partitioning analysis shows that stratiform rainfall is dominant from the morning of 26 July till the late night of 27 July. After that, convective rainfall dominates till about 1000 LST 28 July. Before 28 July, the variations of Q_{WVT} in rainfall-free regions contribute less to that of the domain-mean Q_{WVT} while after that they contribute much, which is consistent to the corresponding variations in their fractional coverage. The variations of Q_{WVF} in rainfall regions are the main contributors to that of the domain-mean Q_{WVF}, then the main contributors to the surface rain rate before the afternoon of 28 July.

Key words: surface rainfall processes; landfalling typhoon; cloud-resolving modeling study

CLC number: P458.1.21 **Document code:** A **doi:** 10.3969/j.issn.1006-8775.2009.02.007

1 INTRODUCTION

China has a very long coast along its eastern and

Received date: 2009-03-28; **revised date:** 2009-09-09

Foundation item: National Basic Research Program of China (973 Program) (2009CB421505); National Natural Science Foundation of China (40775036); Knowledge Innovation Program of Chinese Academy of Sciences (IAP07214)

Biography: CUI Xiao-peng, PhD, professor of meteorology, mainly undertaking the research on mesoscale dynamics, mesoscale and cloud-scale numerical simulations, and surface rainfall processes.

E-mail for correspondence author: xpcui@mail.iap.ac.cn

southern boundaries. During summertime, many typhoons originating in the Western Pacific ocean make landfalls and bring torrential rainfalls and associated social and economical losses over the southeast coast of China and even inland China. Thus typhoon-induced heavy rainfall is always one of the most important topics in the typhoon research community[1-3]. Especially, in 2009, a new National Basic Research Program of China (973 program) was carried out to focus on the abnormal variations during landfalls of typhoons along the coast of China, and one of its main topics is the rainfall associated with landfalling typhoons.

To better understand the surface rainfall and its associated physical processes, Gao et al.[4] derived a diagnostic equation, named surface rainfall equation, in which surface rain rate is simply written as the sum of water vapor and cloud sources/sinks. Hourly cloud-scale simulation data analysis showed that the variations in both water vapor and cloud sources/sinks have important contributions to surface rain rates. Cui and Li[5] further broke the water vapor source/sink term into local vapor change, vapor convergence, and surface evaporation and studied the roles of surface evaporation in tropical surface rainfall processes in both rainfall regions (raining stratiform and convective regions) and rainfall-free regions (non-raining stratiform and clear-sky regions) based on the data from a series of cloud-resolving simulations. Further studies[6-15] showed that the surface rainfall equation[4] is a very useful research tool for analysis of surface rainfall processes.

The understanding of the surface rainfall processes associated with typhoon-induced torrential rainfall and the analysis with the above mentioned surface rainfall equation[4] mainly relies on high-resolution numerical simulations, and Cloud-Resolving Models (CRMs) are a very good choice. CRMs have been widely used to study convective systems and associated rainfall, and to enhance the understanding of physical processes associated with the convective development[11]. CRMs were initially used to study convective responses to imposed large-scale forcings during the convective development within the course of one day. While in the recent years, the models have been utilized to simulate responses of cloud systems under large-scale conditions for week- and even month-long periods.

CRM simulations have been validated with observations in terms of atmospheric thermodynamic states and cloud microphysical and rainfall properties in the tropics during the Global Atmospheric Research Program Atlantic Tropical Experiment (GATE)[16], Tropical Ocean Global Atmosphere Coupled Ocean Atmosphere Response Experiment (TOGA COARE)[17], South China Sea Monsoon Experiment (SCSMEX)[18], and so on. Wang et al.[18] carried out a 2D cloud-resolving simulation during SCSMEX and the simulation was validated with radar observation. The positions of the convective rain, transition zone, and stratiform regions produced by the CRM are consistent with those of the observations. Xu et al.[19] studied a torrential rainfall event over China by using a 2D CRM and validations with observed surface rain rates and radar reflectivities showed good agreement.

In this study, a 2D CRM is used to simulate a torrential rainfall event associated with the landfalling typhoon Kaemi (2006) over the southeast coast of China. The simulation data are validated with rain gauge data and further used to analyze the surface rainfall processes associated with the landfall. Typhoon Kaemi, model, data, experiment, and methodologies are briefly described in the next section. In section 3, the simulation data are validated with observations in the term of surface rain rate. And the surface rainfall processes are analyzed in section 4. Conclusions and discussion are given in the last section.

2 TYPHOON KAEMI, MODEL, DATA, EXPERIMENT, AND METHODOLOGIES OF ANALYSES

Typhoon Kaemi formed in the early morning of 18 July 2006 over the Northwest Pacific ocean. It strengthened into a typhoon in the early morning of 21 July and moved towards the northwest. Kaemi made its first landfall over Taidong of Taiwan province on 2345 LST 24 July 2006 with a maximum wind of 40 m s^{-1} and a minimum center surface pressure of 960 hPa, and made its second landfall over Jinjiang of Fujian province at 1550 25 July 2006 with a maximum wind of 33 ms^{-1} and a minimum center surface pressure of 975 hPa. After that, Kaemi weakened quickly into a tropical storm and then a tropical depression. And after about a 4-day staying over mainland China, Kaemi disappeared over the southern coast of Guangxi province on 29 July 2006. Since it moved very slowly over mainland China, stayed there for more than four days, and moved over several provinces, Kaemi brought heavy rainfalls to most parts of south China, especially Guangdong, Guangxi, Fujian, and Hunan provinces. By interactions with the southwest summer monsoon and the cold air from the north, Kaemi led to the death of more than 60 persons and a direct economical loss of several thousand million RMBs to Hunan, Fujian, Guangdong, Guangxi, Jiangxi, Anhui, and Hubei provinces (from the typhoon yearbook of 2006 of Shanghai Typhoon Institute of China Meteorological Administration).

Fig. 1 shows the large-scale circulations associated with Kaemi. At 0800 LST 24 July, Kaemi was still

over the ocean to the southeast of Taiwan Island. Moist air was transferred continuously from the southwest and the western Pacific Ocean through the southern part of Kaemi's circulation and the passage between the typhoon and the subtropical high (Fig. 1a), and a short trough was located to the northwest of Kaemi at this moment. While there was no apparent direct interaction between the cold air and the warm, moist air associated with the typhoon. At 0800 LST 25 July, Kaemi finished its first landfall on Taidong and was facing the second (Fig. 1b). The main part of the circulation of Kaemi touched the mainland China and the cold air moved towards Kaemi, especially to the west of 110°E. And associated heavy rainfall occurred in the southeast coast of China and the south of China (from the typhoon yearbook of 2006). At this time, the subtropical high moved westwards as the typhoon moved towards the northwest. At 0800 LST 26 July, Kaemi finished its second landfall and weakened into a tropical depression. Its circulation covered most part of the south of China (Fig. 1c) and heavy rainfall mainly occurred in the southern part of the typhoon circulation (from the typhoon yearbook of 2006). From 27 July, Kaemi turned anticlockwise and began to move to the southwest. Heavy rainfall still occurred in the southern part of the typhoon circulation since abundant water vapor was transferred from the summer monsoon circulation (Fig. 1d). Heavy rainfall also occurred in the eastern part of the typhoon circulation since water vapor was also transferred from south to north there (from the typhoon yearbook of 2006). On 28 and 29 July, Kaemi got weaker and moved near to the southern coast of Guangxi. Heavy rainfall mainly occurred close to its coast, and there were also some heavy rainfalls in Guangdong, Fujian, Hunan, and Jiangxi provinces (Fig. 1e, f and the typhoon yearbook of 2006).

The cloud-resolving model used in this study was originally developed by Soong and Ogura, Soong and Tao in 1980. The 2D version of the model, used by Sui et al.[20-21] and further modified by Li et al.[17], is used in this study. The governing equations and model setup can be found in Li et al.[17]. The model includes five prognostic equations for mixing ratios of cloud water, raindrops, cloud ice, snow, and graupel. The cloud microphysical parameterization schemes used in the model are from Rutledge and Hobbs[22-23], Lin et al.[24], Tao et al.[25], and Krueger et al.[26]. The model also includes solar[27] and thermal infrared[28] radiation parameterization schemes that are performed every 3 minutes. Cyclic lateral boundaries are enforced. At the top of the model, a free-slip condition is used for horizontal winds, temperature, and specific humidity, and zero vertical velocity is applied. The horizontal domain is 768 km with a horizontal grid resolution of 1.5 km. The top model level is 42 hPa. The vertical grid resolution ranges from about 200 m near the surface to about 1 km near 100 hPa. The time step is 12 s. Hourly zonal-mean and cloud-partitioned simulation data are used in the analysis. The cloud-resolving model simulations have been validated with observations in terms of atmospheric thermodynamic profiles, surface fluxes, and surface rain rate in the tropics during TOGA COARE[17] and have been applied to study tropical convections[4-9,12,14,15,20,29-33]. A comprehensive model description and results from process studies with this cloud-resolving model can be found in Gao and Li[11].

The model is forced by the imposed zonally-uniform vertical velocity, zonal wind, horizontal temperature and vapor advection from NCEP/GDAS data with a horizontal resolution of 1°× 1° and a temporal resolution of four times per day. The data include geopotential height, temperature, relative humidity, zonal and meridional wind and vertical velocity. The model is integrated from 2000 LST 25 to 1900 LST 31 July 2006 (a total of 6 days) with the large-scale forcing data (Fig. 2) averaged over 23°E – 24°N, 109°E – 116°E (The box in Fig.1).

From Gao et al.[4] and Cui and Li[5], the surface rain rate (P_s) can be expressed as

$$P_s = Q_{WVT} + Q_{WVF} + Q_{WVE} + Q_{CM}, \quad (1)$$

where

$$Q_{WVT} = -\frac{\partial [q_v]}{\partial t}, \quad (1a)$$

$$Q_{WVF} = -[\bar{u}^o \frac{\partial \bar{q}_v^{\,o}}{\partial x}] - [\bar{w}^o \frac{\partial \bar{q}_v}{\partial z}] - [\frac{\partial (u' q_v')}{\partial x}]$$

$$-[\bar{u}^o \frac{\partial q_v'}{\partial x}] - [\bar{w}^o \frac{\partial q_v'}{\partial z}] - [w' \frac{\partial \bar{q}_v}{\partial z}], \quad (1b)$$

$$Q_{WVE} = E_s, \quad (1c)$$

$$Q_{CM} = -\frac{\partial [q_5]}{\partial t} - [\frac{\partial (u q_5)}{\partial x}]. \quad (1d)$$

Here, q_v is specific humidity; u and w are zonal and vertical wind components, respectively; E_s is surface evaporation rate; $q_5 = q_c + q_r + q_i + q_s + q_g$, q_c, q_r, q_i, q_s, q_g are the mixing ratios of cloud water, raindrops, cloud ice, snow, and graupel, respectively; the overbar denotes a zonal-mean; the prime is a perturbation from zonal mean; [ ] is a mass integration; and the superscript "o" is an imposed observed value. Positive values of Q_{WVT}, Q_{WVF}, and Q_{CM} denote local vapor loss, vapor convergence, and local hydrometeor loss/ hydrometeor convergence, respectively, whereas negative Q_{WVT}, Q_{WVF}, and

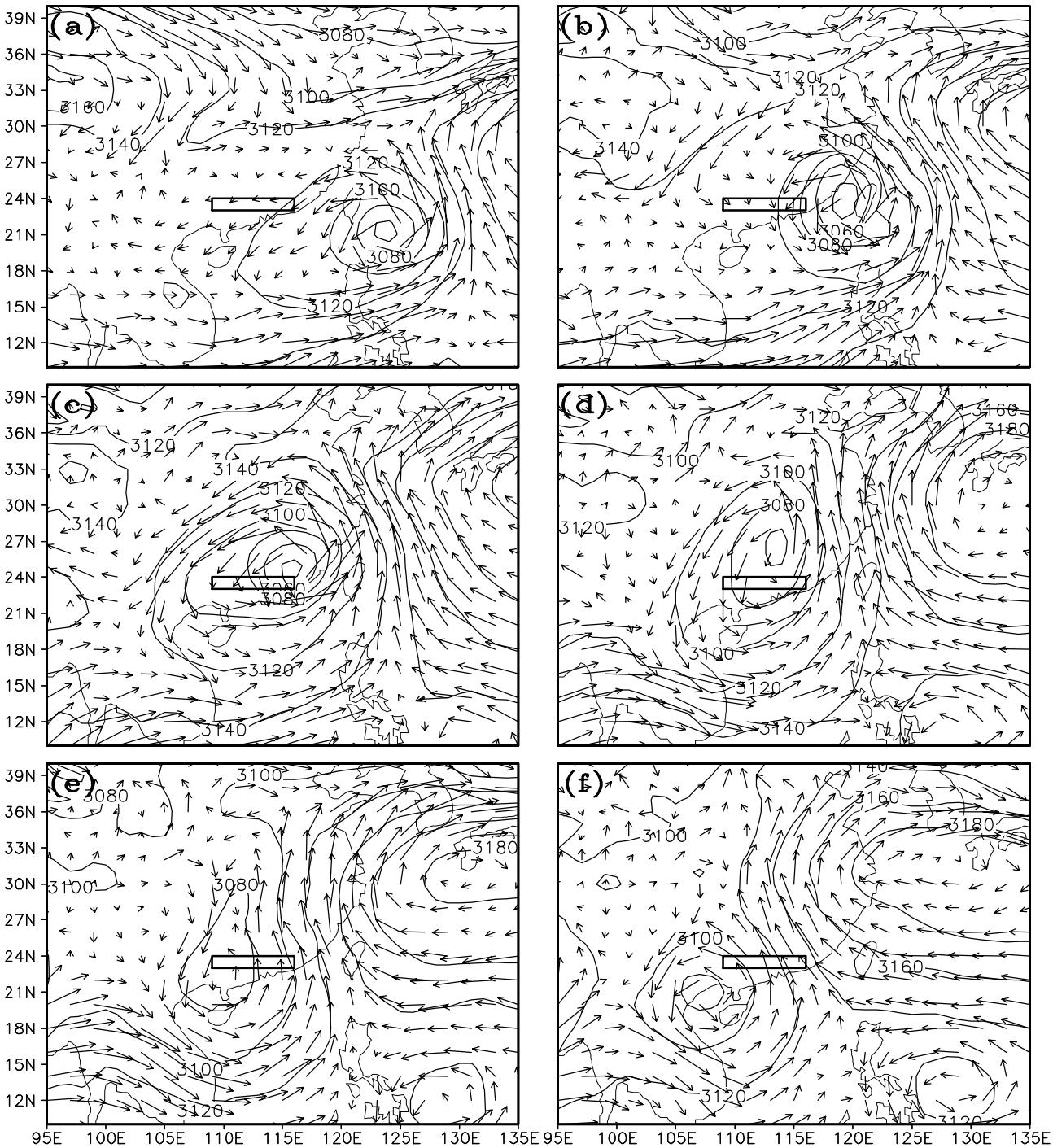

Fig.1 Geopotential height(m) and wind vectors on 700 hPa at (a) 0800 LST 24 July, (b) 0800 LST 25 July, (c) 0800 LST 26 July, (d) 0800 LST 27 July, (e) 0800 LST 28 July, and (f) 0800 LST 29 July.

Q_{CM} denote local vapor gain, vapor divergence, and local hydrometeor gain/hydrometeor divergence, respectively. Surface rain rate is simply expressed as the sum of water vapor source/sink (Q_{WVT}, Q_{WVF}, and Q_{WVE}) and cloud source/sink (Q_{CM}).

To study the surface rainfall processes over different regions, that is, clear sky, raining stratiform, convective, and non-raining stratiform regions, the grid simulation data must be partitioned. Many previous studies have focused on the convective/stratiform cloud partitioning based on the amplitude and spatial variations of radar reflectivity or surface rain rate[34-35]. Additional information like cloud contents, vertical motion, and the fall speed of precipitation particles is also used in partitioning methods[20,36-38]. Here in this study, the partitioning method by Sui et al.[20] is used. In this method, a model grid point is identified as

convective if the rain rate at this grid point is twice as large as the average taken over the surrounding four grid points (two grid points on either side of this grid point in a two-dimensional framework) or a rain rate at this grid point is greater than 20 mm h^{-1}. All non-convective cloudy grid points are considered as stratiform. Additional information with cloud hydrometeors and vertical velocity is used to further detect convective grid points in stratiform regions.

3 COMPARISON OF SIMULATIONS WITH OBSERVATIONS

Kaemi made its second landfall in Jinjiang of Fujian province at 1550 LST on 25 July 2006 and weakened quickly into a tropical storm, and then a tropical depression in the morning the next day. It brought heavy rainfalls to most parts of south China. The main heavy rainfall events occurred from 26 July 2006 and began to dissipate from 28 – 29 July 2006. Fig. 2 shows the large-scale vertical velocity and zonal wind that are imposed in the CRM during the integration. Upward motion was dominant from 26 till 28 July and downward motion began to develop at the higher level of troposphere from the late evening of 28 July.

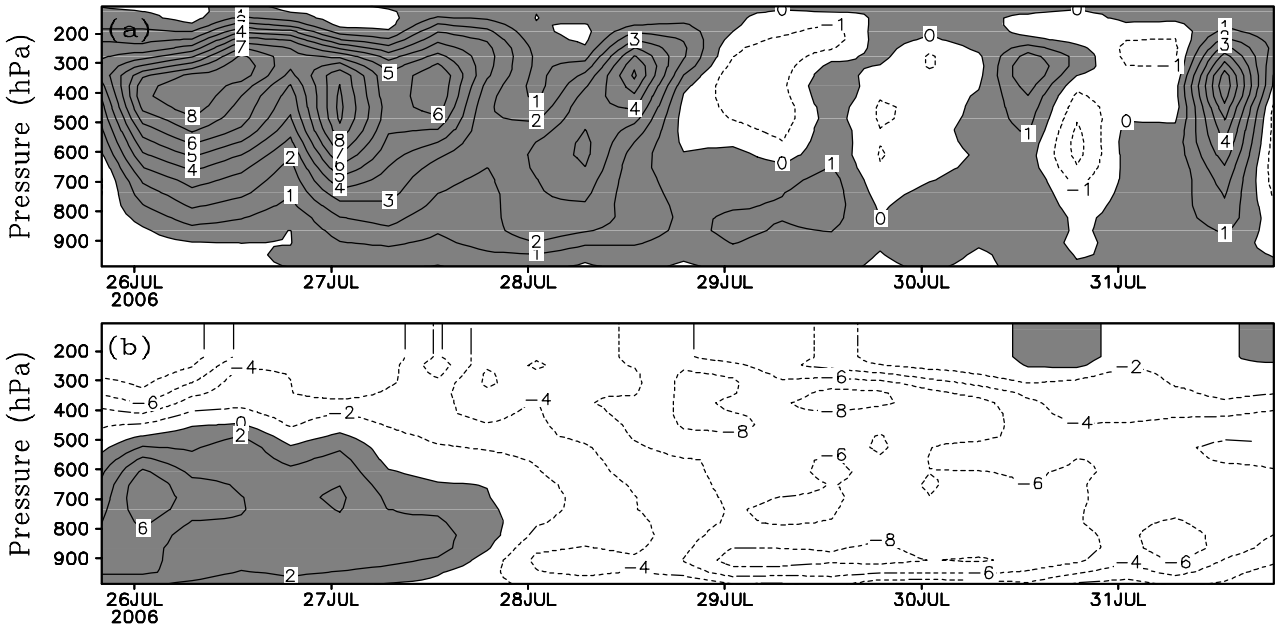

Fig.2 Time-pressure cross sections of (a) vertical velocity (cm s^{-1}) and (b) zonal wind (m s^{-1}) from 2000 LST 25 July to 1900 LST 31 July 2006. The data are averaged in a rectangular box of 23°N – 24°N, 109°E – 116°E. Upward motion in (a) and westerly wind in (b) are shaded.

The time series of model domain-mean simulated surface rain rate is compared with that of the observed surface rain rate in Fig. 3. The observed surface rain rate is calculated by using the rain gauge data in a rectangular box of 23°N – 24°N, 109°E – 116°E, which is the simulation domain and indicated in Fig. 1. The time average of the observed surface rain rate is 0.800 mm h^{-1}, which is very close to the simulated one (0.813 mm h^{-1}). The Root-Mean-Squared (RMS) difference in surface rain rate between the simulation and the gauge observation is 0.660 mm h^{-1}, which is much smaller than the standard deviations of both the simulated rain rate (0.753 mm h^{-1}) and the observed rain rate (0.833 mm h^{-1}). The main differences include: (1) the difference in the first few hours when the integration just starts, which may be caused by the spin-up of the model, (2) the smaller rain rate of the observation around 0000 LST 28 July which is not simulated very well, (3) the shift of rainfall peaks around 1200 LST 30 July, and (4) some missing or underestimated peaks of surface rain rates. The differences may be partially due to the inconsistent calculations of phase and magnitude of the imposed vertical velocity from the 6-hourly NCEP/GDAS data and partially due to the sampling and accuracy of the observed rain gauge data. Nonetheless, the observed and simulated surface rain rates show a very good similarity, especially during the period of 26 – 28 July 2006 (Fig. 3). And the high-resolution grid simulation data could be used in further analysis of surface rainfall processes.

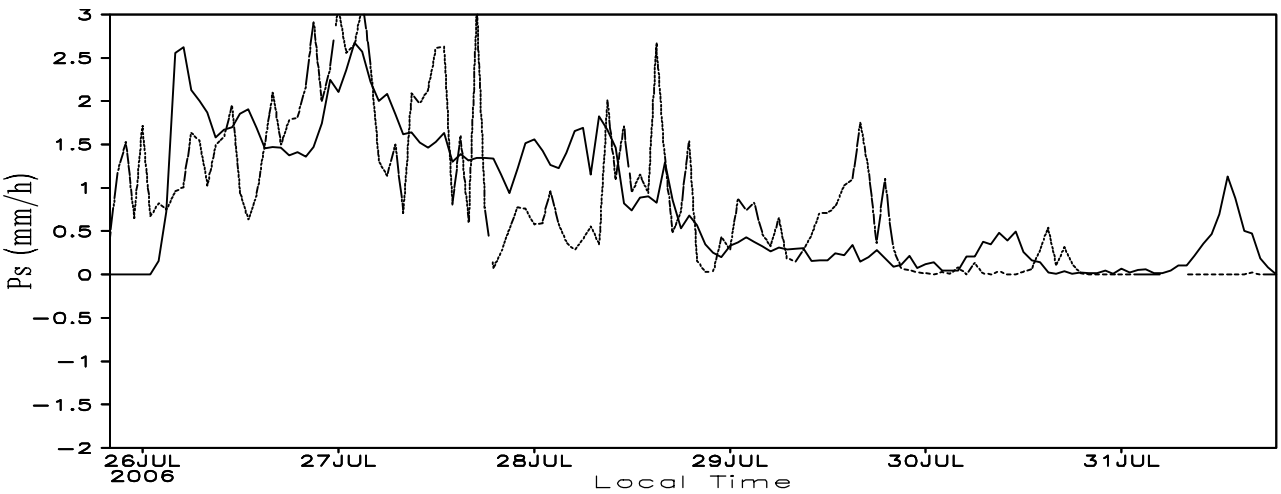

Fig.3 Time series of domain-mean simulated P_s (solid) and observed P_s (dashed) calculated in the rectangular box of 23°N – 24°N, 109°E – 116°E as indicated in Fig. 1. (Unit is mm h^{-1})

4 SURFACE RAINFALL PROCESSES ANALYSIS

4.1 *Model domain mean analysis*

Table 1 gives the time means of fractional coverage, P_s, Q_{WVT}, Q_{WVF}, Q_{WVE}, Q_{CM}, ice water path (*IWP*), and liquid water path (*LWP*), respectively. It shows that time averaged and model domain-mean P_s (0.813 mm h^{-1}) mainly comes from large-scale convergence (Q_{WVF}, 0.665 mm h^{-1}) and local vapor loss (Q_{WVT}, 0.115 mm h^{-1}). Large underestimation (about 15%) of P_s will occur if Q_{WVT} and Q_{CM} are not considered as contributors to P_s (As the methods used in Kuo[39, 40]).

Table 1 Time means of fractional coverage (%), P_s, Q_{WVT}, Q_{WVF}, Q_{WVE}, Q_{CM} (mm h^{-1}), IWP, and LWP (g g^{-1}) over different regions and their sums (model domain-mean).

	Clear-sky regions	Raining stratiform regions	Convective regions	Non-raining stratiform regions	Modeldomain mean
Fractional coverage	38.6	32.4	12.6	16.4	100
P_s	0.000	0.492	0.321	0.000	0.813
Q_{WVT}	-0.001	0.019	0.103	-0.006	0.115
Q_{WVF}	-0.013	0.382	0.289	0.007	0.665
Q_{WVE}	0.012	0.007	0.002	0.005	0.026
Q_{CM}	0.002	0.084	-0.073	-0.006	0.007
IWP	0.000	0.195	0.028	0.024	0.247
LWP	0.000	0.247	0.130	0.008	0.385

Fig. 4 shows the model domain-mean surface rainfall processes analysis by using the above mentioned surface rainfall equation[4-5]. Some features are easy to be noted: (1) Water vapor convergence (Q_{WVF}) accounts for most of the variation of the surface rain rate (P_s) during most of the integration time, while it does not always contribute to P_s, especially after the late night of 28 July, when local vapor loss (positive Q_{WVT}) could be another

contributor to P_s while water vapor divergence (negative Q_{WVF}) restrains P_s. This reveals that surface rainfall could occur even when divergence is dominant; (2) Surface evaporation (Q_{WVE}) is not important to the surface rainfall in this case though it is always positive; (3) Surface rainfall is a result of multi-timescale interactions. Q_{WVE} possesses the longest time scale and the lowest frequency of variation with time, and may exert impacts on P_s on longer time scale[5], and Q_{WVF} possesses the second longest time scale and lowest frequency and can explains most of the variation of P_s. While Q_{WVT} and Q_{CM} possess shorter time scales and higher frequencies which can explain more detailed variations in P_s; (4) Water vapor source/sink (Q_{WVT}, Q_{WVF}, and Q_{WVE}) is the most important contributors to P_s, while sometimes cloud source/sink (Q_{CM}) can also exert important impact[4,15].

4.2 *Partitioning analysis*

To further examine the surface rainfall processes in difference regions, the partitioning method proposed by Sui et al.[20] is applied to each grid point to determine the type (clear sky, raining stratiform, convective, or non-raining stratiform regions) and the summations of quantities are taken and divided by the total zonal grid points (512) for the hourly simulation data.

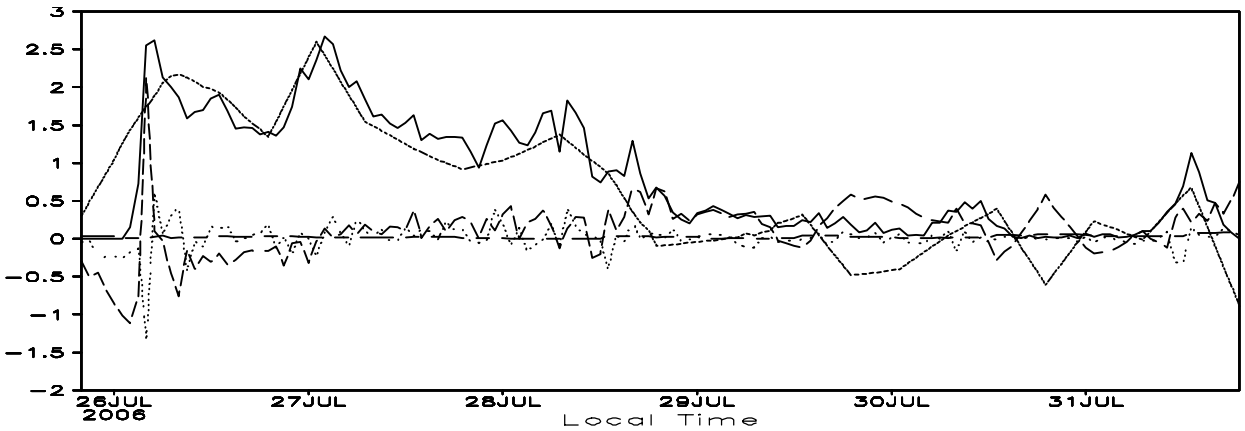

Fig.4 Surface rainfall processes analysis using the surface rainfall equation. The solid, long dashed, dashed, long-short dashed, and dotted lines are referred to as model-domain-mean P_s, Q_{WVT}, Q_{WVF}, Q_{WVE}, and Q_{CM} (mm h^{-1}), respectively.

Table 1 shows the partitioning analysis results. In the 6 days, more than one third (38.6%) of the domain is clear sky, and 45% is occupied by rainfall regions (raining stratiform (32.4%) and convective (12.6%) regions). More than 60% of the surface rain rate (0.813 mm h^{-1}) comes from raining stratiform region (0.492 mm h^{-1}). In raining stratiform region, both water vapor and cloud sources/sinks contribute to surface rain rate, about 78% of the surface rain rate (0.492 mm h^{-1}) comes from water vapor convergence (0.382 mm h^{-1}), and about 17% comes from cloud source/sink (cloud decay, 0.084 mm h^{-1}). In convective region, about one third of the surface rain rate (0.321 mm h^{-1}) comes from local vapor loss (The atmosphere gets drier. 0.103 mm h^{-1}), and water vapor convergence (0.289 mm h^{-1}) contributes to both the other two thirds of the surface rain rate and cloud development (-0.073 mm h^{-1}). This further enhances the important impact of cloud source/sink on surface rainfall processes, and in this case, from the view of time mean and model domain mean, the clear sky and non-raining stratiform regions contribute less.

Fig. 5 shows P_s, Q_{WVT}, Q_{WVF}, Q_{WVE}, Q_{CM}, and fractional coverage in different regions. Partitioning analysis is a very good research tool for understanding detailed surface rainfall processes. In Fig. 5a, stratiform rainfall is dominant from the early morning of 26 July till the late night of 27 July. After that, convective rainfall dominates till about 1000 LST 28 July. Then stratiform rainfall re-dominates till late night of 28 July, and then convective rainfall dominates again till the end of the integration. The variations of Q_{WVT} and Q_{CM} are much complicated during the integration (Fig. 5b, e). Before 28 July, the variations of Q_{WVT} in clear sky and non-raining stratiform

regions contribute less to that of the domain-mean Q_{WVT} while after that they contribute much (Fig. 5b), especially the clear sky, which is consistent with the corresponding variations in their fractional coverage (Fig. 5f) where before 28 July almost the whole domain was occupied by rainfall regions (raining stratiform and convective regions) while after that clear sky region becomes the main contributor and non-raining stratiform region also occupied much of the domain. As for Q_{CM} (Fig. 5e), the variations of Q_{CM} in rainfall regions (raining stratiform and convective regions) are the main contributors to that of the model domain-mean Q_{CM} while the variations of Q_{CM} in rainfall-free regions (clear sky and non-raining stratiform regions) contribute less, especially before 29 July. In Fig.5d, Q_{WVE} are always positive and contribute to the model domain mean in all the four regions, while all Q_{WVE} are too small and contribute less to the surface rain rate on this time scale. Q_{WVF} (Fig. 5c) is the main contributor to the surface rain rate (Fig. 4). The variations of Q_{WVF} in rainfall regions (raining stratiform and convective regions) are the two main contributors to the variations of the model domain-mean Q_{WVF}, then the main contributors to the surface rain rate before the afternoon of 28 July. After that, the contributions from the rainfall-free regions (clear sky and non-raining stratiform regions) get bigger.

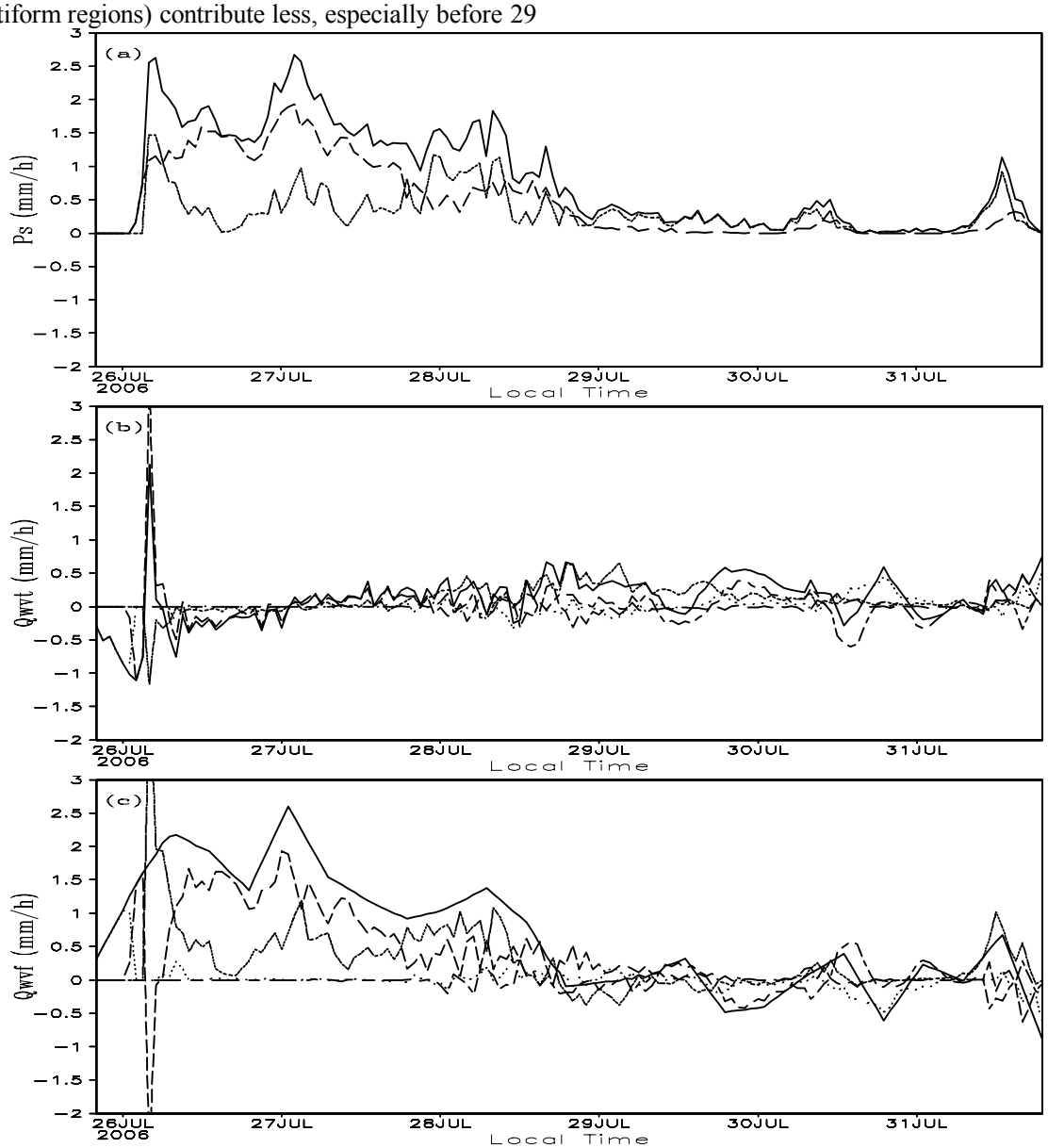

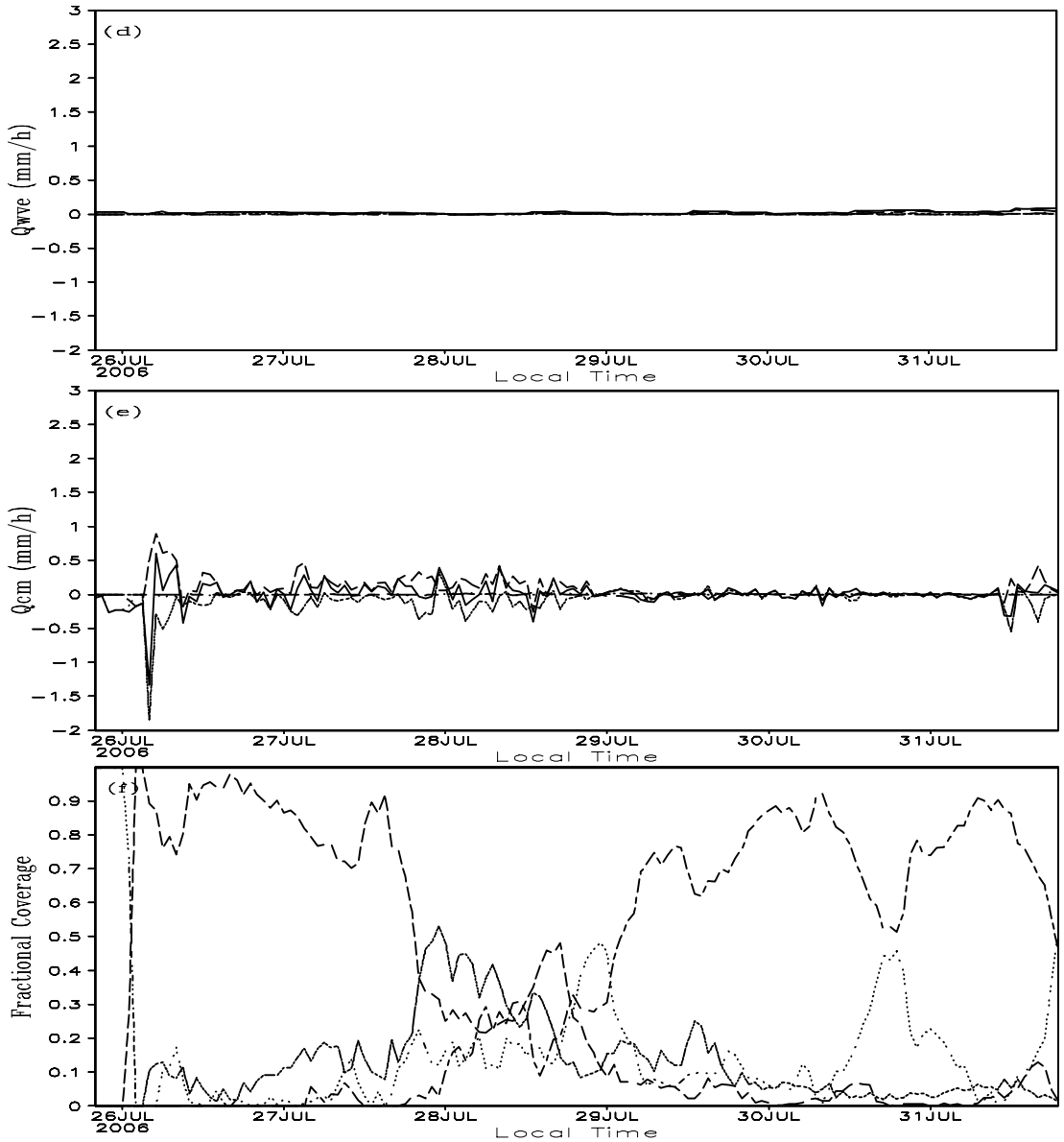

Fig.5 Partitioning analysis. The solid, long-short dashed, long dashed, dashed, and dotted lines are referred to model domain mean, clear sky, raining stratiform, convective, and non-raining stratiform regions, respectively. (a) P_s, (b) Q_{WVT}, (c) Q_{WVF} ,(d) Q_{WVE} ,(e) Q_{CM} and (f) fractional coverage. (Units for a-e: mm h^{-1})

5 CONCLUSIONS AND DISCUSSION

China has a very long coast and many typhoons can make landfalls during summertime and bring torrential rainfalls and social and economical losses to China. To better understand the surface rainfall processes associated with landfalling typhoons over China, a case typhoon, Kaemi (2006), is selected and the corresponding detailed surface rainfall processes are investigated based on hourly data from a 2D CRM simulation and the surface rainfall equation[4,5].

The model is integrated for 6 days with imposed large-scale forcing calculated from NCEP/GDAS data. The simulation data are validated with observations in terms of surface rain rates. The Root-Mean-Squared (RMS) difference in surface rain rates between the simulation and the gauge observations is 0.660 mm h^{-1}, which is much smaller than the standard deviations of both the simulated rain rate (0.753 mm h^{-1}) and the observed rain rate (0.833 mm h^{-1}).

The simulation data are then used to study the physical causes associated with the surface rainfall processes during the landfall. The results show that time averaged and model domain-mean P_s mainly comes from large-scale convergence (Q_{WVF}) and local vapor loss (positive Q_{WVT}). Large underestimation (about 15%) of P_s will occur if Q_{WVT} and Q_{CM}

are not considered as contributors to P_s (As in Kuo[39, 40]). Q_{WVF} accounts for the variation of P_s during most of the integration time, while it does not always contribute to P_s. Sometimes local vapor loss (positive Q_{WVT}) could be another contributor to P_s while water vapor divergence (negative Q_{WVF}) restrains P_s. This tells that surface rainfall could occur when divergence is dominant. Surface rainfall is a result of multi-timescale interactions. Q_{WVE} possesses the longest time scale and the lowest frequency of variation with time, and may exert impact on P_s on longer time scale, and Q_{WVF} possesses the second longest time scale and lowest frequency and can explain most of the variation of P_s. While Q_{WVT} and Q_{CM} possess shorter time scales and higher frequencies which can explain more detailed variations in P_s.

Partitioning analysis tells that stratiform rainfall is dominant from the morning of 26 July till the late night of 27 July. After that, convective rainfall dominates till about 1000 LST 28 July. Before 28 July, the variations of Q_{WVT} in rainfall-free regions contribute less to that of the model domain mean while after that they contribute much, which is consistent with the corresponding variations in their fractional coverage. Q_{WVF} is the main contributor to the surface rain rate. The variations of Q_{WVF} in rainfall regions are the two main contributors to the variations of the model domain-mean Q_{WVF}, then the main contributors to the surface rain rate before the afternoon of 28 July. After that, the contributions from the rainfall-free regions get bigger.

In the future, more details about the surface rainfall processes associated with Typhoon Kaemi, such as microphysical budgets, will be analyzed based on the simulation data and the surface rainfall equation.

REFERENCES:

[1] CHEN Lian-shou, LUO Zhe-xian, LI Ying. Research advances on tropical cyclone landfall process [J]. Acta Meteor. Sinica (in Chinese), 2004, 62(5): 541-549.

[2] ZHANG Hai-xia, CUI Xiao-peng, KANG Feng-qin, et al. Observational analysis for a torrential rain caused by a landfall typhoon [J]. Plateau Meteor. (in Chinese), 2007, 26(5): 980-991.

[3] ZHAO Yu, CUI Xiao-peng, WANG Jian-guo. A study on a heavy rainfall event triggered by inverted typhoon trough in Shandong province [J]. Acta Meteor. Sinica (in Chinese), 2008, 66(3): 423-436.

[4] GAO S T, CUI X P, ZHU Y S, et al. Surface rainfall processes as simulated in a cloud resolving model [J]. J. Geophys. Res., 2005, 110, D10202, doi: 10.1029/2004JD005467.

[5] CUI X P, LI X F. Role of surface evaporation in surface rainfall processes [J]. J. Geophys. Res., 2006, 111, D17112, doi: 10.1029/2005JD006876.

[6] GAO S T, PING F, LI X F. Cloud microphysical processes associated with the diurnal variations of tropical convection: A 2D cloud resolving modeling study [J]. Meteor. Atmos. Phys., 2006, 91: 9-16.

[7] GAO S T, PING F, CUI X P, et al. Short timescale air-sea coupling in the tropical deep convective regime [J]. Meteor. Atmos. Phys., 2006, 93: 37-44.

[8] GAO S T. A three dimensional dynamic vorticity vector associated with tropical oceanic convection [J]. J. Geophys. Res., 2007, 113, doi: 10.1029/2006JD008247.

[9] CUI X P, ZHOU Y S, LI X F. Cloud Microphysical Properties in Tropical Convective and Stratiform Regions [J]. Meteor. Atmos. Phys., 2007, 98: 1-11.

[10] SUI C H, LI X F, YANG M J. On the definition of precipitation efficiency [J]. J. Atmos. Sci., 2007, 64(12): 4506-4513.

[11] GAO S T, LI X F. Cloud-resolving modeling of convective processes [M]. 2008, Dordrecht: Springer, 206 pp.

[12] CUI X P. A Cloud-Resolving Modeling Study of Diurnal Variations of Tropical Convective and Stratiform Rainfall [J]. J. Geophys. Res., 2008, 113, D02113, doi: 10.1029/2007JD008990.

[13] CUI Xiao-peng, LI Xiao-fan, ZONG Zhi-ping. Cloud microphysical and Rainfall Responses to Zonal Perturbations of Sea Surface Temperature: A Cloud-Resolving Modeling Study [J]. Prog. Nat. Sci., 2009, 19(5): 587-594.

[14] GAO Shou-ting, CUI Xiao-peng, LI Xiao-fan. A modeling Study of Diurnal Rainfall Variations during the 21-Day Period of TOGA COARE [J]. Adv. Atmos. Sci., 2009, 26(5): 895-905.

[15] CUI Xiao-peng. Quantitative diagnostic analysis of surface rainfall processes by surface rainfall equation [J]. Chin. J. Atmos. Sci. (in Chinese), 2009, 33(2): 375-387.

[16] GRABOWSKI W W, WU X Q, MONCRIEFF M W. Cloud-resolving model of tropical cloud systems during Phase III of GATE. Part I: Two dimensional experiments [J]. J. Atmos. Sci., 1996, 53(24): 3684-3709.

[17] LI X F, SUI C H, LAU K M, et al. Large-scale forcing and cloud-radiation interaction in the tropical deep convective regime [J]. J. Atmos. Sci., 1999, 56(17): 3028-3042.

[18] WANG J J, LI X F, CAREY L. Evolution, structure, cloud microphysical and surface rainfall processes of a monsoon convection during the South China Sea Monsoon Experiment [J]. J. Atmos. Sci., 2007, 64(2): 360-380.

[19] XU X F, XU F W, LI B. A cloud-resolving modeling study of a torrential rainfall event over China [J]. J. Geophys. Res., 2007, 112, D17204, doi: 10.1029/2006JD008275.

[20] SUI C H, LAU K M, TAO W K, et al. The tropical water and energy cycles in a cumulus ensemble model. Part I: Equilibrium climate [J]. J. Atmos. Sci., 1994, 51(5): 711-728.

[21] SUI C H, LI X F, LAU K M. Radiative-convective processes in simulated diurnal variations of tropical oceanic convection [J]. J. Atmos. Sci., 1998, 55(13): 2345-2357.

[22] RUTLEDGE S A, HOBBS P V. The mesoscale and microscale structure and organization of clouds and

precipitation in midlatitude cyclones. Part VIII: A model for the "seeder-feeder" process in warm-frontal rainbands [J]. J. Atmos. Sci., 1983, 40(5): 1185-1206.
[23] RUTLEDGE S A, HOBBS P V. The mesoscale and microscale structure and organization of clouds and precipitation in midlatitude cyclones. Part XII: A diagnostic modeling study of precipitation development in narrow cold-frontal rainbands [J]. J. Atmos. Sci., 1984, 41(20): 2949-2972.
[24] LIN Y L, FARLEY R D, ORVILLE H D. Bulk parameterization of the snow field in a cloud model [J]. J. Appl. Meteor., 1983, 22(6): 1065-1092.
[25] TAO W K, SIMPSON J, MCCUMBER M. An ice-water saturation adjustment [J]. Mon. Wea. Rev., 1989, 117(1): 231-235.
[26] KRUEGER S K, FU Q, LIOU K N, et al. Improvement of an ice-phase microphysics parameterization for use in numerical simulations of tropical convection [J]. J. Appl. Meteor., 1995, 34(1): 281-287.
[27] CHOU M D, SUAREZ M J, HO C H, et al. Parameterizations for cloud overlapping and shortwave single scattering properties for use in general circulation and cloud ensemble models [J]. J. Climate, 1998, 11(2)**:** 202-214.
[28] CHOU M D, KRATZ D P, RIDGWAY W. Infrared radiation parameterization in numerical climate models [J]. J. Climate, 1991, 4(4): 424-437.
[29] CUI Xiao-peng. A phase analysis of vorticity vectors associated with tropical convection [J]. Chin. Phys., 2008, 17(6): 2304-2307.
[30] CUI Xiao-peng, GAO Shou-ting. Effects of zonal perturbations of sea surface temperature on tropical equilibrium states: A cloud-resolving modeling study [J]. Prog. Nat. Sci., 2008, 18(4): 413-419.
[31] GAO S T, CUI X P, ZHOU Y S, et al. A Modeling study of moist and dynamic vorticity vectors associated with 2d tropical convection [J]. J. Geophys. Res., 2005, 110, D17104, doi: 10.1029/2004JD005675.
[32] GAO Shou-ting, CUI Xiao-peng, LI Xiao-fan. A modeling study of relation between cloud amount and SST over western tropical Pacific cloudy regions during TOGA COARE [J]. Prog. Nat. Sci., 2009, 19(2): 187-193.
[33] GAO S T, PIN F, LI X F, et al. A convective vorticity vector associated with tropical convection: A two-dimensional cloud-resolving modeling study [J]. J. Geophys. Res., 2004, 109, D14106, doi: 10.1029/2004JD004807.
[34] CANIAUX G, REDELSPERGER J L, LAFORE J P. A numerical study of the stratiform region of a fast-moving squall line. Part I: General description and water and heat budgets [J]. J. Atmos. Sci., 1994, 51(14): 2046-2074.
[35] STEINER M, HOUZE R A, YUTER S E. Climatological characterization of three-dimensional storm structure from operational radar and rain gauge data [J]. J. Appl. Meteor., 1995, 34(9): 1978-2007.
[36] TAO W K, LANG S, SIMPSON J, et al. Retrieval algorithms for estimating the vertical profiles of latent heat release: Their applications for TRMM [J]. J. Meteor. Soc. Japan, 1993, 71(6): 685-700.
[37] XU K M. Partitioning mass, heat, and moisture budgets of explicitly simulated cumulus ensembles into convective and stratiform components [J]. J. Atmos. Sci., 1995, 52(5): 551-573.
[38] LANG S, TAO W K, SIMPSON J, et al. Modeling of convective-stratiform precipitation processes: Sensitivity to partition methods [J]. J. Appl. Meteor., 2003, 42(4): 505-527.
[39] KUO H L. On formation and intensification of tropical cyclones through latent heat release by cumulus convection [J]. J. Atmos. Sci., 1965, 22(1): 40-63.
[40] KUO H L. Further studies of the parameterization of the influence of cumulus convection on large-scale flow [J]. J. Atmos. Sci., 1974, 31(5): 1232-1240.

Citation: CUI Xiao-peng and XU Feng-wen. A cloud-resolving modeling study of surface rainfall processes associated with landfalling typhoon Kaemi(2006). *J. Trop. Meteor.*, 2009, 15(2): 181-191.